Direct Probing of the Spatial Distribution of the Maximum Josephson Current in a Superconducting Tunnel Junction

J. Bosch, R. Gross, M. Koyanagi,[a] and R. P. Huebener
Physikalisches Institut II, Universität Tübingen, D-7400 Tübingen, Federal Republic of Germany
(Received 26 December 1984)

We report the first experimental results obtained by low-temperature scanning-electron microscopy on the spatial distribution of the maximum Josephson current in tunnel junctions. The experiments were performed with a nearly one-dimensional PbIn-PbBi window junction, its length being large compared to λ_J. The spatial resolution is 1–2 μm and is governed by the thermal healing length. In a parallel magnetic field the different vortex states have been clearly observed. The nonlocal effects due to the beam-induced change of the phase-difference function predicted by Chang *et al.* have also been confirmed.

PACS numbers: 74.50.+r, 07.80.+x, 61.16.Di

Low-temperature scanning electron microscopy (LTSEM) represents a highly promising method for investigating structures in superconducting thin films and Josephson tunnel junctions.[1,2] Recently we have applied this technique for studying hotspots in thin-film superconductors[3] and the quasiparticle current-density distribution in superconducting tunnel junctions.[4-6] In this paper we report the first experimental results on the spatial distribution of the maximum Josephson current density in superconducting tunnel junctions obtained by LTSEM. Using a long one-dimensional tunnel junction (in-line geometry) in a parallel magnetic field we have clearly observed up to twelve vortices, our spatial resolution being 1–2 μm. The nonlocal effects due to the beam-induced change of the relative pair phase reflecting the macroscopic quantum properties of the junction and predicted by Chang and co-workers[7-9] also have been clearly detected.

The dominant effect of electron-beam irradiation in a thin-film superconductor is a localized increase of the quasiparticle and phonon number density near the coordinate point of the beam focus. In the limit of high phonon trapping, appropriate for our case, electron-beam irradiation can be treated as a simple heating effect,[10] since there is local thermal equilibrium between the quasiparticles and the phonons. For the one-dimensional junction geometry shown in Fig. 1 and with y as the coordinate in the direction of the longest junction dimension, the density of the maximum Josephson current is

$$J(y)=J_1(y)\sin\Phi(y). \tag{1}$$

Here J_1 is the local critical-current density and Φ the phase-difference function. The local perturbation of the junction by the electron beam is expected to change the critical-current density J_1 in the irradiated region. If the phase-difference function Φ were to remain unaffected, the measured beam-induced change $\Delta I_1(y)$ of the junction critical current as a function of the beam position would be proportional to the current distribution in the unperturbed junction biased at its critical-current value. In this way, simple direct imaging of the critical-current distribution would be possible.

However, as pointed out by Chang, and co-workers,[7-9] the beam-induced change in the phase-difference function Φ cannot be ignored in general and can have a significant effect on the measured quantity $\Delta I_1(y)$. The change in the function Φ results from the increase in the London penetration depth λ_L and in the Josephson screening length λ_J due to the beam irradiation. The effective range of the phase disturbance is determined by the Josephson screening length which is large compared to the diameter of the area perturbed by the electron beam. Therefore, local irradiation of the tunnel junction causes a change ΔI_1 of the total critical current which includes both a change of the amplitude J_1 of the critical current density and a change of the phase-difference function Φ. The influence of the electron beam on the critical-current density is a local effect whereas its influence on the phase-difference function is a nonlocal effect resulting from the macroscopic quantum properties of the Josephson junction. In the limit of weak perturbation, the beam-induced change ΔI_1 can be separated into two parts[8]:

$$\Delta I_1=\Delta I_J+\Delta I_\Phi, \tag{2}$$

with

$$\Delta I_J=\int dy\,\Delta J_1(y)\sin\Phi(y) \tag{3}$$

and

$$\Delta I_\Phi=\int dy\,J_1(y)\cos\Phi(y)\Delta\Phi(y). \tag{4}$$

Here J_1 and Φ are the unperturbed critical-current density and critical phase-difference function, respectively. The quantities $\Delta J_1(y)$ and $\Delta\Phi(y)$ are the corresponding beam-induced changes. Because of the local nature of ΔJ_1, ΔI_J has the same spatial dependence

as the unperturbed current density $J_1(y)\sin\Phi(y)$. However, ΔI_Φ can be quite complicated.

The principle of our experiment is shown schematically in Fig. 1. The electron beam is scanned over the surface of the junction and the beam-induced change of the maximum Josephson current is measured as a function of the beam position. The substrate carrying the junction is mounted on the low-temperature stage of the scanning-electron microscope so that the junction is exposed to the vacuum of the sample chamber and can be irradiated directly with the electron beam, whereas the backside of the substrate is in direct contact with the liquid-helium bath.[11] A magnetic field parallel to the junction barrier could be applied by passing an electric current through the upper electrode only, as indicated in Fig. 1. All experiments were performed at the bath temperature $T_b = 4.2$ K.

The planar thin-film tunnel junctions were evaporated on a single-crystal sapphire substrate of 1-mm thickness and 20-mm diameter. Before evaporation the sapphire substrate was partly coated with a Nb-ground plane of 1500-Å thickness and a SiO insulating layer of 3300-Å thickness. The samples were in-line window junctions where the tunneling area was given by an opening in a thin insulating SiO layer deposited on the base electrode. The base electrode was a PbIn film of 1300-Å thickness. A PbBi film of 3300-Å thickness served as the counter electrode. The rectangular tunneling barrier of about 3.5×90-μm^2 area was formed by oxidation of the base electrode in a O_2 atmosphere at room temperature. The dimensions of the junction have been chosen such that the width was smaller and the length L much larger than the Josephson penetration depth λ_J. As indicated by quasiparticle current distribution obtained from our voltage-imaging method,[4-6] the tunneling barrier of the junction for which the following results were obtained was reasonably homogeneous.

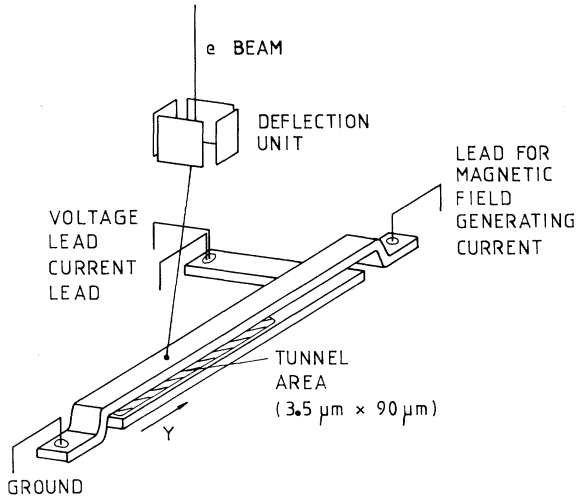

FIG. 1. Principle of the experiment.

The important quantity to be measured is the change ΔI_c produced in the critical current by the beam irradiation as a function of the coordinates of the beam focus. The critical current was measured using an electronic ramp generator increasing the sample current until a nonzero voltage appeared. This critical current was stored in a sample-and-hold unit by means of a corresponding voltage value. From the output of this unit a voltage signal proportional to $-\Delta I_c$ was generated. This measuring process was repeated with a frequency in the range of 1–10 kHz. Two-dimensional images of ΔI_c were obtained by linearly scanning the electron beam several times over the sample and shifting the individual scans transversely in small steps. Simultaneously the voltage signal proportional to $-\Delta I_c$ was fed to the deflection unit of the display screen by using the y-modulation mode of the SEM. During a linear scan over a length of 100 μm, the critical current was measured about 10^4–10^5 times. In this way the recording time for the image such as that shown in Fig. 3 is typically about 1 min. During our experiments the beam parameters were 26-kV voltage and about 10-pA current. We note that this imaging method is distinctly different from the voltage-imaging technique we have developed for displaying the quasi-particle current distribution.[4-6]

In Fig. 2 we show part of the magnetic interference pattern obtained for the junction used in the scanning

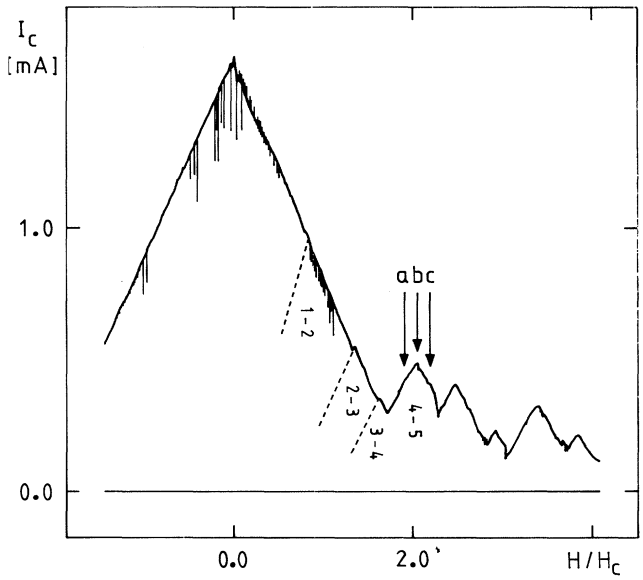

FIG. 2. Magnetic interference pattern: maximum Josephson current vs the reduced magnetic field. The regions for the different vortex states are indicated. The arrows a–c indicate the field values at which the recordings shown in Fig. 3 were obtained.

experiments. The pattern is typical for a junction with a length $L >> \lambda_J$. The critical field H_c is given by

$$H_c = \frac{\hbar c}{2ed\lambda_J}, \quad (5)$$

where d is the effective thickness of the barrier. At low fields the linear decrease of the critical current due to Meissner screening is clearly exhibited. Further, the overlapping of the different vortex states can be seen. The lower vortex states are difficult to distinguish in the interference pattern due to the overlap. Their existence is indicated only by noise (1–2 vortex state) or a small peak (2–3 vortex state). Only the modes containing 4–5 vortices and the higher vortex modes are clearly exhibited. We will show below that the different vortex states in the magnetic interference pattern can clearly be identified from the images of the current distribution. The measurements of the interference pattern were extended also to larger negative field values than shown in Fig. 2. The pattern was found to be highly symmetric for positive and negative fields, indicating only a negligible influence of the Nb-ground plane (which appears reasonable in view of the 3300-Å separation between ground plane and base electrode).

In Fig. 3 we show typical recordings of the signal $-\Delta I_c(y)$ obtained by scanning over the junction area along the y direction for different values of the transverse coordinate. The junction position and the scanning direction are indicated in Fig. 3(d). The patterns shown in Figs. 3(a)–3(c) were obtained at the magnetic field values indicated in Fig. 2 by the corresponding arrows. In this field range the 4–5 vortex state is established, as clearly demonstrated by the recordings. In Fig. 3(b) the maximum amplitudes of the beam-induced change $-\Delta I_c(y)$ correspond to about 160 μA, i.e., to about 30% of the maximum critical current shown in Fig. 2 for this state. The data shown in Figs. 3(a) and 3(c) were obtained on the low- and high-field side of the interference maximum, respectively. Here the nonlocal junction response due to the influence of the phase-difference function Φ can clearly be seen. As calculated by Chang and coworkers,[7–9] this nonlocal effect causes a variation of the amplitudes of the oscillation in $\Delta I_c(y)$ along the y coordinate. In particular, they predict that the amplitudes are an increasing (decreasing) function of y for $dI_c/dH > 0$ ($dI_c/dH < 0$), in good agreement with our results. The theoretical results presented in Fig. 2 of Ref. 8 for the case of a long nearly one-dimensional junction with $L/\lambda_J = 10$ are most pertinent to our experimental case. The recordings shown in Fig. 3(b) were obtained for the field value $H/H_c = 2.08$ close to the maximum critical current of this vortex state where $dI_c/dH = 0$. In this case the theory predicts that the amplitudes of the oscillation are uniform[8,9] in agreement with our experimental data.

Figure 4 shows the recordings obtained at higher magnetic fields for the 10–11 vortex state near its maximum critical current. Again, the spatial variation

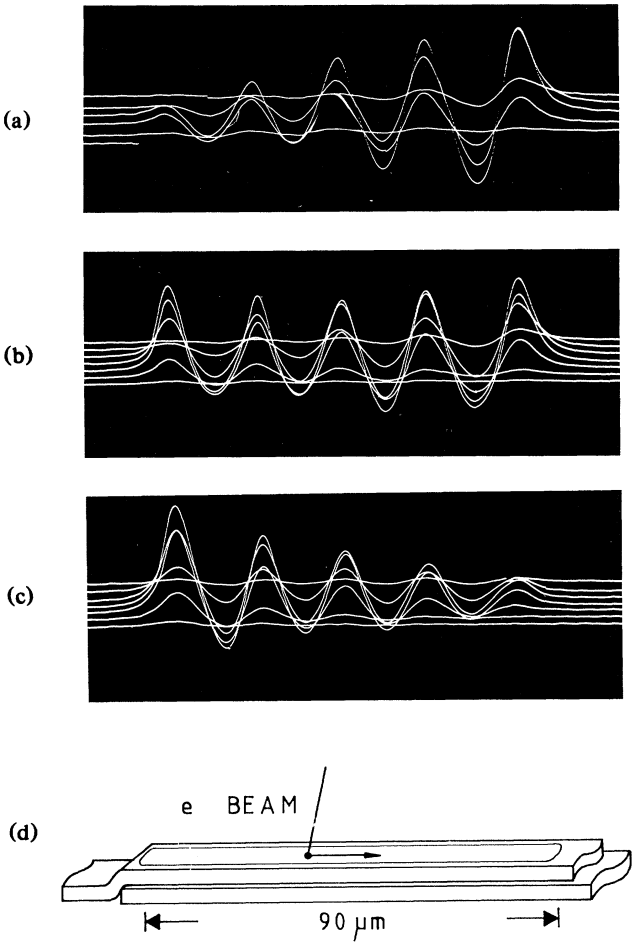

FIG. 3. The signal $-\Delta I_c(y)$ showing the 4–5 vortex state obtained by scanning longitudinally along the junction area. The position of the junction and the scanning direction are shown at the bottom. (a)–(c) Recordings obtained at the reduced fields marked in Fig. 2 by the corresponding arrows.

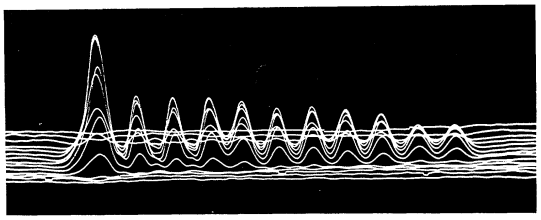

FIG. 4. The signal $-\Delta I_c(y)$ showing the 10–11 vortex state obtained by scanning longitudinally along the junction area.

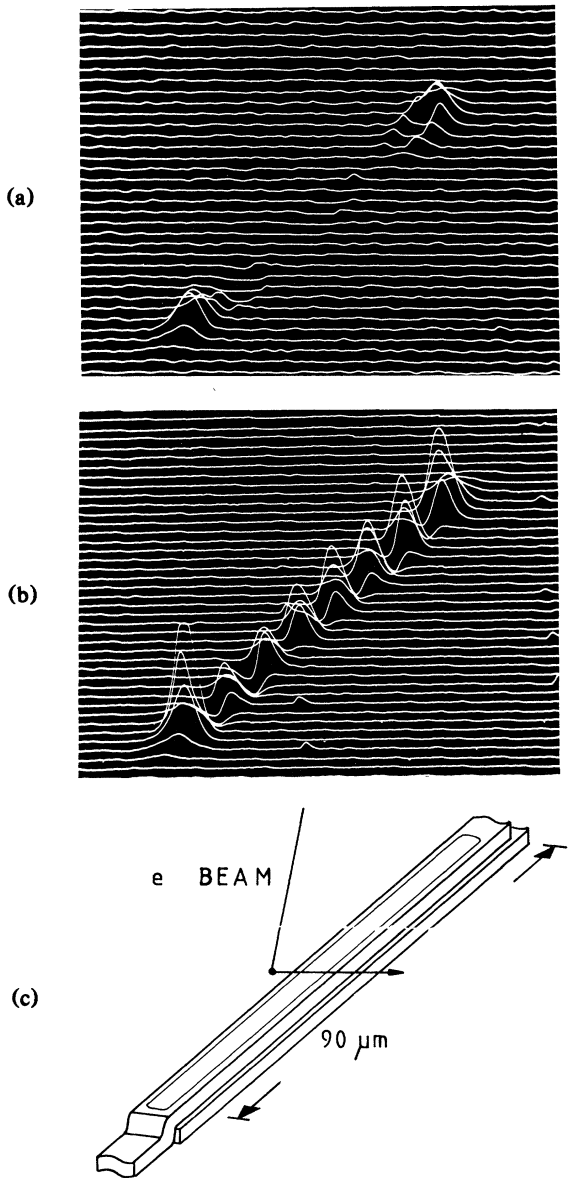

FIG. 5. The signal $-\Delta I_c$ obtained by scanning transversely across the junction area. The position of the junction and the scanning direction are shown at the bottom. (a) $H/H_c \approx 0$; (b) the 7–8 vortex state for $H/H_c = -3.98$.

of the amplitudes due to the nonlocal effects can be seen. The high spatial resolution of this imaging method is demonstrated by the clear appearance of the individual vortices.

In order to check that the images were not affected by the scanning direction, we have scanned along different directions. The images shown in Fig. 5 were obtained by scanning in transverse direction across the junction as indicated at the bottom. Figure 5(a) shows the image for $H/H_c \approx 0$ and clearly exhibits the self-field effect. Figure 5(b) shows the 7–8 vortex state for $H/H_c = -3.98$. In general the same results were found for the longitudinal and transverse scanning direction.

It is interesting to compare our results with those recently obtained[12,13] using a laser-scanning technique which is conceptually similar to our method. The spatial resolution in their experiments is determined by the spot size of the laser beam ranging between 20 and 80 μm.[13] Due to the small diameter of the electron beam (about 0.1 μm), the resolution of our scanning method is at least an order of magnitude higher than that obtained previously by laser-beam scanning.[12,13]

Valuable discussions and assistance provided by H. Seifert in the beginning of this work are gratefully acknowledged. This work was supported in part by the Alexander von Humboldt-Stiftung and by the Stiftung Volkswagenwerk.

[a]Permanent address: Electrotechnical Laboratory, 1-1-4 Umezono, Sakura-Mura, Niiharigun, Ibaraki, Japan.

[1]J. R. Clem and R. P. Huebener, J. Appl. Phys. **51**, 2764 (1980).

[2]R. P. Huebener, Rep. Prog. Phys. **47**, 175 (1984).

[3]R. Eichele, L. Freytag, H. Seifert, R. P. Heubener, and J. R. Clem, J. Low Temp. Phys. **52**, 449 (1983).

[4]P. W. Epperlein, H. Seifert, and R. P. Huebener, Phys. Lett. **92A**, 146 (1982).

[5]H. Seifert, R. P. Huebener, and P. W. Epperlein, Phys. Lett. **95A**, 326 (1983).

[6]H. Seifert, R. P. Huebener, and P. W. Epperlein, Phys. Lett. **97A**, 421 (1983).

[7]J. J. Chang and D. J. Scalapino, Phys. Rev. B **29**, 2843 (1984).

[8]J. J. Chang and C. H. Ho, Appl. Phys. Lett. **45**, 182 (1984).

[9]J. J. Chang, C. H. Ho, and D. J. Scalapino, to be published.

[10]R. Gross and M. Koyanagi, to be published.

[11]H. Seifert, Cryogenics **22**, 756 (1982).

[12]M. Scheuermann, J. R. Lhota, P. K. Kuo, and J. T. Chen, Phys. Rev. Lett. **50**, 74 (1983).

[13]J. R. Lhota, M. Scheuermann, P. K. Kuo, and J. T. Chen, Appl. Phys. Lett. **44**, 255 (1983).